Biomaterials xxx (2011) 1–12

Contents lists available at ScienceDirect

Biomaterials

journal homepage: www.elsevier.com/locate/biomaterials

Microstructure design of biodegradable scaffold and its effect on tissue regeneration

Yuhang Chen, Shiwei Zhou, Qing Li*

School of Aerospace, Mechanical and Mechatronic Engineering, The University of Sydney, New South Wales 2006, Australia

ARTICLE INFO

Article history:
Received 9 March 2011
Accepted 28 March 2011
Available online xxx

Keywords:
Biodegradation
Tissue ingrowth
Mechanobiology
Homogenization
Topology optimization
poly(lactic-co-glycolic acid) (PLGA)

ABSTRACT

Biodegradable scaffolds play a critical role in therapeutic tissue engineering, in which the matrix degradation and tissue ingrowth are of particular importance for determining the ongoing performance of tissue-scaffold system during regenerative process. This paper aims to explore the mechanobiological process within biodegradable scaffolds, where the representative volume element (RVE) is extracted from periodic scaffold micro-architectures as a base-cell design model. The degradation of scaffold matrix is modeled in terms of a stochastic hydrolysis process enhanced by diffusion-controlled autocatalysis; and the tissue ingrowth is modeled through the mechano-regulatory theory. By using the finite element based homogenization technique and topology optimization approach, the effective properties of various periodic scaffold structures are obtained. To explore the effect of scaffold design on the mechanobiological evolutions of tissue-scaffold systems, different scaffold architectures are considered for polymer degradation and tissue regeneration. It is found that the different tissues can grow into the degraded voids inside the polymer matrix. It is demonstrated that the design of scaffold architecture has a considerable impact on the tissue regeneration outcome, which exhibits the importance of implementing different criteria in scaffold micro-structural design, before being fabricated via rapid prototyping technique, e.g. solid free-form fabrication (SFF). This study models such an interactive process of scaffold degradation and tissue growth, thereby providing some new insights into design of biodegradable scaffold micro-architecture for tissue engineering.

1. Introduction

Biodegradable scaffolds, as key artificial devices widely used in tissue engineering, aim to provide a desirable micro-environment that allows neo-tissue to be generated properly for repairing and replacing damaged tissues or organs. As a fundamental premise in tissue engineering, scaffold should provide (a) host-tissue-like mechanical support for promoting neo-tissue growth and functioning [1]; (b) adequate porosity and permeability for nutrient delivery and metabolite removal [2]; and (c) a controllable degradation rate of scaffold matrix [3]. To assess these design requirements, substantial experimental studies have been conducted to explore the *in vivo* and *in vitro* behaviors for a range of porous scaffolds [4–7].

To improve the performance of tissue scaffolds, various material parameters, e.g. stiffness, porosity and permeability, have proven particularly crucial to determine the biomechanical environments within scaffold micro-architectures [5,8,9]. However, the optimal values of these parameters have not been consistently available yet [10]. On the one hand, increasing scaffold stiffness could lead to a potential decrease in porosity and permeability, which prevents the neo-tissue from proper ingrowth to the bulk of scaffolds. On the other hand, increasing scaffold porosity might lead to a higher permeability but the effective stiffness would be sacrificed. To compromise these competing criteria, multi-objective design optimization is essential to seek optimal scaffold architectures for promoting overall biological performance of scaffold. Following the success of topology optimization methods [11], increasing work has been carried out to develop various optimal scaffold architectures [12–15]. Nevertheless, for biodegradable scaffold, an initial optimal design may not guarantee the ideal characteristics due to continuous material degradation and neo-tissue ingrowth. It would be interesting to understand how the dynamic chemical (matrix degradation) and biological (tissue regeneration) evolutions affect the effective properties of scaffold architecture over the healing time.

Biodegradation is one of the key factors to determine the time-dependent performance of scaffolds. It has been recognized that there are two categories of polymeric degradation. The first is named as 'surface' erosion, in which the degradation occurs mainly on the surface in contact with surrounding liquid, while the second

* Corresponding author. Tel.: +61 2 9351 8607; fax: +61 2 9351 7060.
E-mail address: Qing.Li@Sydney.edu.au (Q. Li).

0142-9612/$ – see front matter © 2011 Elsevier Ltd. All rights reserved.
doi:10.1016/j.biomaterials.2011.03.064

is named 'bulk' degradation that takes place throughout the whole material domain [16]. For some materials, e.g. sebacic acid (SA) and 1,3-bis(*p*-carboxyphenoxy)propane (CPP) the former dominates, while for some other materials (e.g. poly(lactic acid) (PLA) and poly(lactic-co-glycolic acid) (PLGA)) the latter dominates [17].

Although the concept that scaffolding material is expected to gradually disappear over time has been widely accepted, how to quantify the effect of degradation on tissue growth and how to control the degradation process to achieve the optimal regeneration outcome is still rather challenging [18,19]. The mechanical properties required by the host-tissue can be one of the most important criteria for scaffold micro-architectural design, whereas the degradation continuously decomposes polymer matrix and reduces the structural stiffness and strength, which may lead to a premature destruction or mechanical failure of scaffold. More importantly, for such commonly-used biodegradable polymers as PLA and PLGA, the hydroxyl end groups released from hydrolysis reaction can diffuse within the polymer matrix, which in turn increase the local hydrolysis rate substantially, thus making the degradation size-dependent (the hydrolysis rate in the bulk of polymer matrix is higher than the surface rate) [20–22]. Such size-effect could essentially alter the degradation pathway and dynamically change the mechanical environment within scaffold structure [22]. It is therefore crucial to understand how the matrix degradation affects the biomechanical capability of tissue-scaffold system for better promoting the regeneration outcome.

Mechanobiology, as a concept that biological process is regulated by mechanical signals, has attracted increasing attention over the recent years [23,24]. It is believed that biophysical stimulus plays a key role in regulating the tissue growth and remodeling process [25,26], which seems fairly promising in studying bone fracture healing [27,28] and tissue regeneration in porous scaffolds [29,30]. The mechano-regulatory model adopts mechanical strain and fluid flow to modulate cell differentiation and has shown considerable potential to capture the growth details of various cell phenotypes under different levels of biophysical stimuli [31]. Further developed by Byrne et al. [32], this method allows conducting the analyses in two different length scales: one in the scaffold level where mechanical and fluidic fields were analyzed through the poroelasticity model; the other one in cellular level where the proliferation and differentiation of mesenchymal stem cells (MSCs) were simulated based on the correlation between the levels of mechano-regulatory stimuli and experimental data. More recently, Stops et al. [33] also used this model to predict the cell response to mechanical fields within a collagen–glycosaminoglycan scaffold. Furthermore, vascularization was modeled by a lattice-based mechanobiological approach [34]. However, it remains unclear how the scaffold architecture and degradation could continuously alter the mechanical environment and consequently determine the tissue regeneration outcome.

This paper aims to explore the performance of different scaffold designs by assessing their capacities of stimulating neo-tissue growth in a biodegradation framework. Throughout this study, representative volume element (RVE) is extracted from scaffold as the design model, in which the periodic boundary conditions are applied to mimic the periodicity of scaffold micro-structure. A series of scaffold architectures are first designed in the RVE scale by using a multi-objective topology optimization procedure. A newly developed degradation model [22], in which the stochastic hydrolysis process is enhanced by the diffusion-controlled autocatalysis, is adopted here. The scaffold subject to continuous degradation will further undergo the mechano-regulatory tissue regeneration model. As such, a time-dependent process of scaffold degradation and tissue ingrowth is modeled, which allows characterizing the dynamic evolutions of effective stiffness and permeability of tissue-scaffold systems by using the homogenization technique, thereby exploring the effect of scaffold micro-architectural design on tissue regeneration.

2. Methods

As the rapid development of solid free-form fabrication (SFF) technology [35], periodic scaffold architectures that comprise multiple base-cells (RVEs) attract significant attention due to their more controllable effective properties. In this paper, we would like to restrain our attention on this class of scaffold architectures; though the degradation and tissue ingrowth models are also applicable to other scaffolds consisted of random micro-structures.

2.1. Homogenization method and topology optimization formulation

From the structural point of view, the base-cell of scaffold micro-architecture typically has a much smaller length scale (~0.1–0.3 mm) than its macro-structure (~10–30 mm), with a size ratio around 100 or more. While *in-vitro* experiments showed that the biochemical environment of each base cell may differ from one location to other under a static condition, a relatively uniform environment can be created across all the base-cells, from boundary to core, under a proper dynamic condition [36], making the periodic 'base-cell model' applicable for tissue engineering. As a result, the homogenization technique can be employed to estimate the effective properties from the base-cell model. Specifically, the discretized form of effective (bulk or macroscopic properties of entire micro-architectural structure) elasticity and permeability can be expressed as [37]

$$C^H_{ijkl} = \frac{1}{|\Omega|}\sum_{e=1}^{NE}|\Omega^e|[\mathbf{u}^e_0(\varepsilon^0_{ij}) - \mathbf{u}^e(\varepsilon^*_{ij})]^T\mathbf{k}^e(\rho^e)[\mathbf{u}^e_o(\varepsilon^0_{kl}) - \mathbf{u}^e(\varepsilon^*_{kl})] \quad (1)$$

$$P^H_{ij} = \frac{1}{|\Omega|}\sum_{e=1}^{NE}|\Omega^e|(\mathbf{v}^e_i)^T\mathbf{p}^e(\rho^e)(\mathbf{v}^e_j) \quad (2)$$

where C^H_{ijkl} and P^H_{ij} are the effective elasticity and permeability tensors; $\mathbf{k}^e(\rho^e)$ and $\mathbf{p}^e(\rho^e)$ are the local stiffness and permeability matrices of element e as the functions of elemental density ρ^e (the fundamental design variable) [11]; $\mathbf{u}^e_0(\varepsilon^0_{ij})$ and $\mathbf{u}^e(\varepsilon^*_{ij})$ are the nodal displacements associated with the unit test strain ε^0 and fluctuation strain field ε^*_{ij}, respectively. $\mathbf{v}^e_i$ denotes the nodal velocity yielded from the stable Stokes flow solution [37]. Eqs. (1) and (2) allow assessing the effective (macroscopic) properties of materials directly from the base-cell (RVE) model (or namely the '*direct*' homogenization) [38].

To seek an optimal scaffold architecture for the stiffness and permeability criteria, a multi-objective topology optimization in terms of an *inverse* homogenization procedure can be applied [14,39], as

$$\min J(\rho^e) = w_s f_s + w_p f_p = \sum_{e=1}^{NE}\left[w_s\frac{C^*}{\sum_{i,j}^{6}\delta_{ij}C^H_{ij}} + w_p\frac{P^*}{\sum_{i,j}^{3}\delta_{ij}P^H_{ij}}\right] \quad (3)$$

$$s.t.\sum_{e=1}^{NE}V^e\rho^e = V_c; 0 \le \rho_{\min} \le \rho^e \le 1; w_s + w_p = 1; i,j\epsilon[x,y,z]$$

where J denotes an aggregate objective function, and f_s and f_p are the stiffness and permeability objective functions, respectively. δ_{ij} is the kronecker delta ($\delta_{ij} = 1$ when $i = j$ and $\delta_{ij} = 0$ when $i \neq j$). V_c is the constraint of volume fraction and $\rho_{\min}$ denotes the minimum density to avoid numerical singularity in finite element analysis. Weighting factors w_s and w_p are used to regulate the relative importance of stiffness and permeability criteria in the design. C^* and P^* are the normalizing parameters for both criteria and also used to generate the multi-objective Pareto front [40]. C^H_{ij} and P^H_{ij} are the effective stiffness and permeability tensors that represent the mechanical and fluidic properties for the entire scaffold structure, respectively, and can take the following matrix forms after introducing orthotropy,

$$C^H_{ij} = \begin{bmatrix} C_{xx} & C_{xy} & C_{xz} & 0 & 0 & 0 \\ C_{yx} & C_{xy} & C_{yz} & 0 & 0 & 0 \\ C_{zx} & C_{zy} & C_{zz} & 0 & 0 & 0 \\ 0 & 0 & 0 & G_{yz} & 0 & 0 \\ 0 & 0 & 0 & 0 & G_{xz} & 0 \\ 0 & 0 & 0 & 0 & 0 & G_{xy} \end{bmatrix}; P^H_{ij} = \begin{bmatrix} P_x & 0 & 0 \\ 0 & P_y & 0 \\ 0 & 0 & P_z \end{bmatrix} \quad (4)$$

For the symmetrical effective stiffness tensor C^H_{ij}, six diagonal values represent three normal components (C_{xx}, C_{yy}, C_{zz}) and three shear components (G_{xy}, G_{yz}, G_{xz}), respectively, which are the most vital parameters for reflecting mechanical characteristics of scaffold structure (the other six off-diagonal elements that contain Poisson's ratios v_{ij} are not discussed in this study); For the effective permeability tensor P^H_{ij}, only the components along the orthogonal axes are considered since the shear permeable moduli are extremely (often 10^{-10} times) lower in fluid than in solid [41]. Following the topology optimization problem defined in Eq. (3) (i.e. from

Please cite this article in press as: Chen Y, et al., Microstructure design of biodegradable scaffold and its effect on tissue regeneration, Biomaterials (2011), doi:10.1016/j.biomaterials.2011.03.064

the extremal or desirable effective properties of materials to inversely design the RVE micro-structure [14,39]), different micro-architectures of scaffold can be obtained by adjusting w_s and w_p, providing fairly distinct combinations of effective stiffness and permeability properties.

2.2. Degradation model

Let us consider a biodegradable polymer matrix that is uniformly discretized into a number of degradation elements to represent three different statuses of 'hydrolysable' ($\chi_H = 1$), 'hydrolyzed' ($\chi_h = 0.001$) and 'void' ($\chi_v = 0$). It is assumed that, the size distribution and density of polymer chains are approximately uniform throughout the scaffold matrix as long as the number of elements is sufficiently large. Variable χ can be thus viewed as either the normalized average molecular weight or mass of local polymer matrix [22]. The scaffold matrix is assumed to be fully immersed in water at the initial state ($t = 0$). When the water molecules attack the chain bonds, hydrolysis reaction takes place. The normalized molecular weight loss can be modeled in a first-order kinetic process [42], as

$$M_a^l = 1 - e^{-\lambda t} \tag{5}$$

where λ is the degradation rate constant that can be determined by a linear regression of known experimental data [43]. Based on the established stochastic degradation theory [42], the time-dependent average molecular weight loss of M_a^l can be predicted by the first-order Erlang stochastic process [44]. In the scaffold scenarios, there is substantial volume of initial pore space, which makes the probability density function $P(\lambda,t)$ be calculated as [22]

$$P(\lambda, t) = \frac{\lambda e^{-\lambda t}}{V_0 V(t)} \tag{6}$$

where V_0 and $V(t)$ are the volume fractions of polymer matrix at time 0 and t, respectively. Note that $V(t)$ compensates the reduction of volume fraction due to degradation for calculating $P(\lambda,t)$. For each run of determining the hydrolysis state (variable χ) for a hydrolysable element, a random number between 0 and 1 is generated. If the random number is less than $P(\lambda,t)$, this element is considered to be hydrolyzed and its state variable χ becomes 0.001 at the following time step. In contrast, if the random number is greater than $P(\lambda,t)$, this element remains unchanged and will participate in the stochastic hydrolysis in the following steps.

The *in vitro* tests have demonstrated that the acid byproducts generated from hydrolysis reaction of some commonly-used biodegradable polymers, e.g. PLA and PLGA, are hydrolytic catalysts. Such an autocatalysis effect can accelerate local hydrolysis reaction, thus affecting the degradation rate of scaffold [45,46]. To account for this effect, the concentration of hydrolyzed monomers C_m is calculated as

$$C_{mnew}^N = C_m^N + \frac{\chi_H - \chi_h}{n} \tag{7}$$

where C_m^N and C_{mnew}^N are the nodal values of C_m in a degraded element before and after the hydrolysis reaction, respectively, and n is the number of nodes for a single degradation element. After the monomers and oligomers are released from the hydrolysis reaction inside the polymer, the diffusion of these components is determined by the Fick's second law,

$$\frac{\partial C_m}{\partial t} = \nabla(D_m \nabla C_m) + S(t) \tag{8}$$

where D_m is the diffusivity of degraded products depending on the extent of local hydrolysis as $D_m = D_M^0 e^{R_m(\chi_H - \chi)/\chi_H}$ (here D_M^0 is the diffusivity prior to hydrolysis and R_m is a material constant [47]), and $S(t)$ is the source term of released monomers generated by the hydrolysis reaction.

As a result, we consider the final degradation process in twofold: (1) a fundamental hydrolysis without autocatalysis; (2) an accelerating effect due to autocatalysis governed by the diffusion of interior acid catalyst. According to the studies by Lam et al. [46] and von Burkersroda et al. [16], the autocatalysis follows an exponential relation to the fundamental hydrolysis. Thus the total accelerated probability density function P_A can be formulated as

$$P_A = P_F + P_c = P_F + \beta\left(e^{C_m} - 1\right) P_F = \frac{\lambda_0 e^{-\lambda_0 t}}{V_0 V_{(t)}}[1 + \beta(e^{C_m} - 1)] \tag{9}$$

where P_F and P_C are the probability components due to the fundamental hydrolysis and autocatalysis, respectively. λ_0 is an autocatalysis-free degradation rate constant. As stated above, the extent of autocatalysis is governed by a diffusion process, which largely depends on the size and configuration of polymeric device, implying the importance of scaffold design. Note that autocatalysis parameter β plays a role in regulating the autocatalysis contribution, which allows us to better match the modeling result to the known experimental data. For the detailed description and the examples on drug delivery microparticles and scaffolds of the degradation model used herein, interested readers are referred to our recent paper [22].

2.3. The mechano-regulatory tissue regeneration model

In tissue engineering, scaffold provides a proper biomechanical environment and certain level of biophysical stimulus for promoting MSCs differentiation. Based on the aforementioned scaffold architectures obtained from the topological design in Eq. (3), the mechano-regulatory tissue regeneration model is introduced herein. The pore region in the scaffold is considered to be occupied by granulation tissue after a certain period of culturing in bioreactor, in which the lattices are constructed within each granulation element as a cellular media, allowing various cell phenotypes to potentially occupy. The number of lattice points is determined by the size of element and average diameter of tissue cells. In the beginning, we seeded 5% MSCs into each lattice in the mathematical model. In other words, MSCs are randomly seeded at 5% of the lattice points inside the scaffold pore, which are allowed to further proliferate and differentiate. To account for the cell proliferation and migration, the random walk algorithm [32] is adopted in this study.

Having defined the cell proliferation and migration in the '*lattice scale*', the relationship between local physical fields and MSC differentiation stimulus S can be defined from the mechano-regulatory model as proposed in [31], as

$$S = \frac{\tau}{a} + \frac{v}{b} \begin{cases} S < 0.01 & \text{absorption} \\ 0.01 < S < 0.53 & \text{osteoblast} \rightarrow \text{mature bone} \\ 0.53 < S < 1 & \text{osteoblast} \rightarrow \text{immature bone} \\ 1 < S < 3 & \text{chondrocyte} \rightarrow \text{cartilage} \\ S > 3 & \text{fibroblast} \rightarrow \text{fibrous tissue} \end{cases} \tag{10}$$

where τ and v are octahedral shear strain and fluidic velocity within the base-cell of tissue-scaffold construct, respectively. Following the literature, constants a=0.0375 and b=3 μms^{-1} that were obtained from experiments are adopted to generate biophysical stimulus S for differentiation [48]. It is assumed that each MSC has duration of 7 days [32], after which it becomes mature to be able to proliferate or differentiate. Thus, different cell phenotypes would be differentiated from MSCs according to the calculated biophysical stimulus S in Eq. (10), where only a certain percentage of mature MSCs in each lattice, defined by a differentiation probability p_d, differentiates every day. To calculate material properties in each lattice, we adopted the material parameters of different cell phenotypes and the algorithm reported by Byrne et al. [32].

Following the scaffold degradation, some new voids are generated inside the scaffold matrix, thereafter neo-tissue may grow into such voids if nutrients and metabolites can diffuse through. Note that the MSCs proliferation and differentiation are dependent on the local oxygen and nutrition concentrations, it is thus hypothesized that MSCs directly connected to the original scaffold pores (where the oxygen and nutrition are considered to be sufficient) or an adjacent pre-connected element are activated and keep participating in the mechano-regulatory regeneration process. At the initial stage ($t = 0$), originally-designed pore space of scaffold is fully occupied by granulation tissue; and the nutrition therein is considered to be sufficient. When the hydrolysis takes place, it is assumed that more and more polymeric elements degrade and will possibly be replaced by the granulation substances. As such, the MSCs can migrate and proliferate into the degraded voids in the scaffold structure and continuously differentiate into neo-tissues there.

3. Results and discussion

In this study, a 50:50 PLGA is used as the matrix material of scaffolds in the following examples. The autocatalysis-free degradation rate constant λ_0, initial diffusivity of degraded products D_m^0 and materials constant R_m are set as 0.02 day^{-1}, 0.53 $\times$ 10^{-7} mm^2/s and 7.69, respectively [22,47,49]. The size of RVE in each dimension is chosen as 1 mm. From the previous study, β is set as 1 to address the autocatalysis effect [22]. Each element is considered to have 6 lattice points in the x, y and z directions, respectively. The differentiation probability p_d of mature MSCs is set as 0.3 for each iteration (day) [32]. In order to generate the physiological mechanical stimulus, two rigid plates are placed at one pair of surfaces in the base-cell model. Although a specific value of physiological compressive pressure has not been firmly known yet and sometimes even differs from individual to individual, tissue to tissue, and scaffold to scaffold, the compressive loading in general functional status of cancellous bone is in a range of 0.5–10 MPa [50]. Meanwhile, as suggested in literature [51], 1 MPa external pressure is applied along the y axis in 2D models and the x axis in 3D models as the external mechanical stimulus in this study.

The diffusion-reaction polymer degradation and physical fields for calculating the stimulus S are computed in the element-level of base-cell model, while the mechano-regulatory MSC proliferation

Please cite this article in press as: Chen Y, et al., Microstructure design of biodegradable scaffold and its effect on tissue regeneration, Biomaterials (2011), doi:10.1016/j.biomaterials.2011.03.064

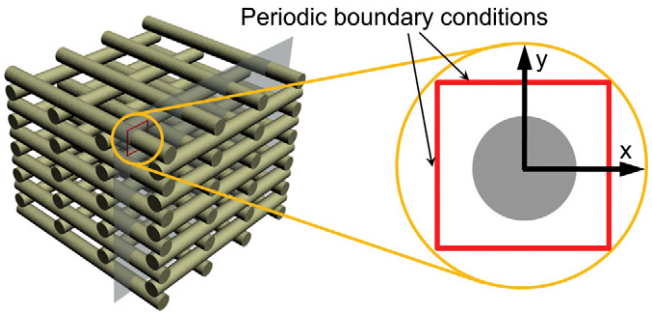

Fig. 1. Schematic diagram of PLGA scaffold in strut frame. An RVE of cross-sectional configuration is chosen as the region of interest (red domain), where periodic boundary conditions are applied on the RVE boundaries to mimic the periodicity of scaffold.(For interpretation of the references to colour in this figure legend, the reader is referred to the web version of this article.)

and differentiation are calculated in the lattice-level. The homogenization method is used here to estimate the effective (bulk or macroscopic) properties of entire tissue-scaffold system (i.e. multi-RVEs structure) from the base-cell model.

3.1. 2D models: scaffold in strut framework

As the first example, the scaffolds in strut framework that are fabricated by the fused deposition modeling (FDM) technique are used in this section [52]. An RVE of cross-sectional configuration in scaffold strut network is chosen as the region of interest, as illustrated in Fig. 1, where the periodic boundary conditions are applied to mimic the micro-architectural periodicity. In order to show the effect of scaffold architecture on tissue regeneration, two representative groups of tests are carried out herein. The first group includes two scaffolds that have circular and rectangular cross-sectional shapes of rods with 80% porosity; and the second group contains the scaffolds that have the circular cross-section but different porosities of 80%, 65% and 50%, respectively.

Fig. 2 shows the tissue ingrowth in scaffolds with rectangular and circular configurations, respectively. At the early stage (day 15), the fibrous tissue starts to generate adjacent to the interface of scaffold matrix (dark region in the upper-left and right schematic diagrams) in the both cases due to a higher shear strain therein, while the cartilage forms an 'X'-shaped pattern. As the scaffold degrades, more neo-tissue is found in the core region which gradually fills the void of hydrolyzed elements inside the scaffold matrix. It is observed that after 60 days the tissue-scaffold systems in both cases become stable when the majority of polymer matrix completes its degradation and the newly-formed tissue becomes mature. Regarding the tissue ingrowth inside the degraded voids of scaffold matrix, the formation of neo-tissue exhibits considerably random characteristics due to the stochastic nature of degradation model. However, since the mechanical stiffness of scaffold strut is much higher than that of granulation tissue, most of MSCs that migrate and proliferate inside the matrix may differentiate into osteoblasts due to a lower shear strain therein, potentially forming the bony tissue in the due course.

To further investigate the effect of scaffold design on tissue regeneration, two other cases with 50% and 65% porosity are also presented, as illustrated in Fig. 3. It can be seen that, apart from the region of polymer matrix, the patterns of neo-tissue generation in these three different cases fairly resemble due to the similar mechanical and fluidic fields (the two key contributors for

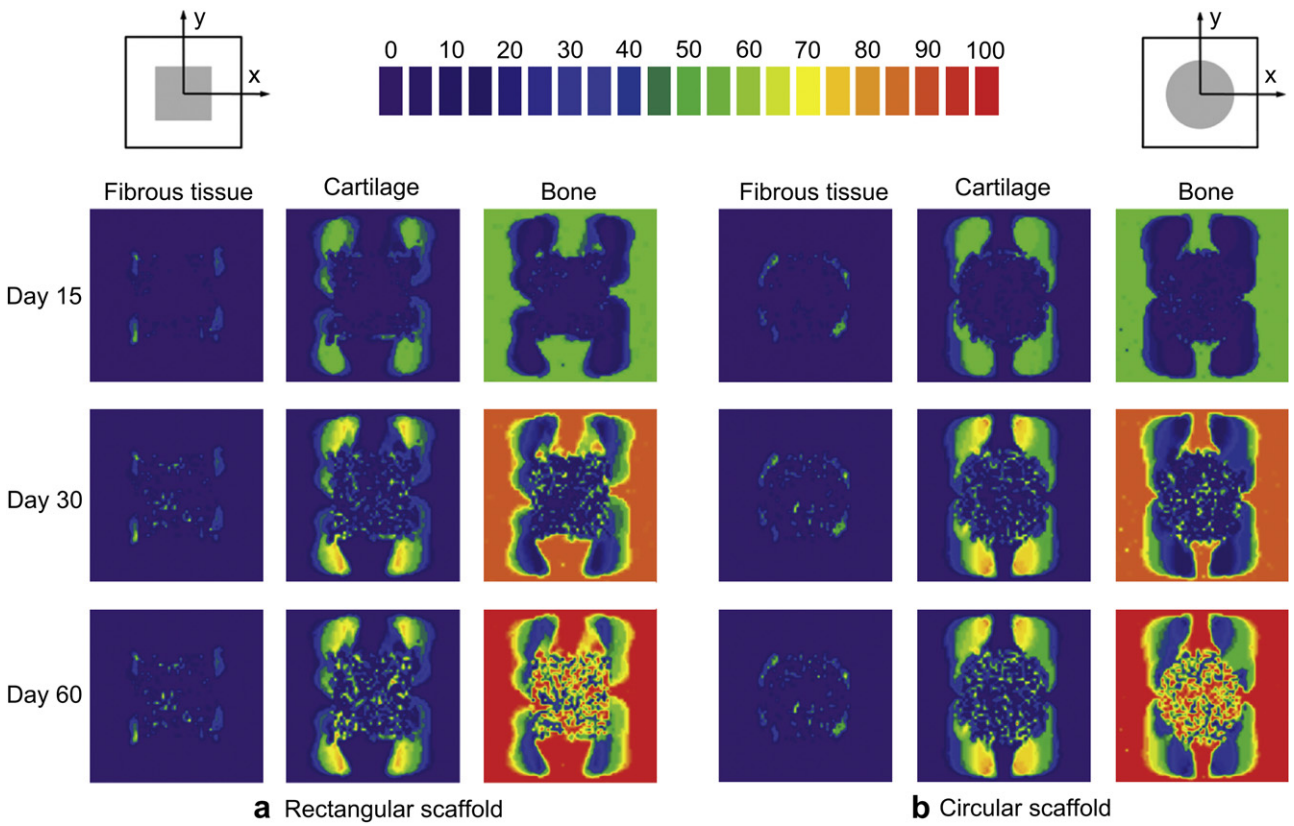

Fig. 2. The mechanobiological evolutions of PLGA scaffold in the strut frames (porosity = 80%). Upper-left and right schematic diagrams shows the configuration of scaffold RVE (dark region represents polymer matrix). (a) Rectangular cross-section. (b) Circular cross-section.

Please cite this article in press as: Chen Y, et al., Microstructure design of biodegradable scaffold and its effect on tissue regeneration, Biomaterials (2011), doi:10.1016/j.biomaterials.2011.03.064

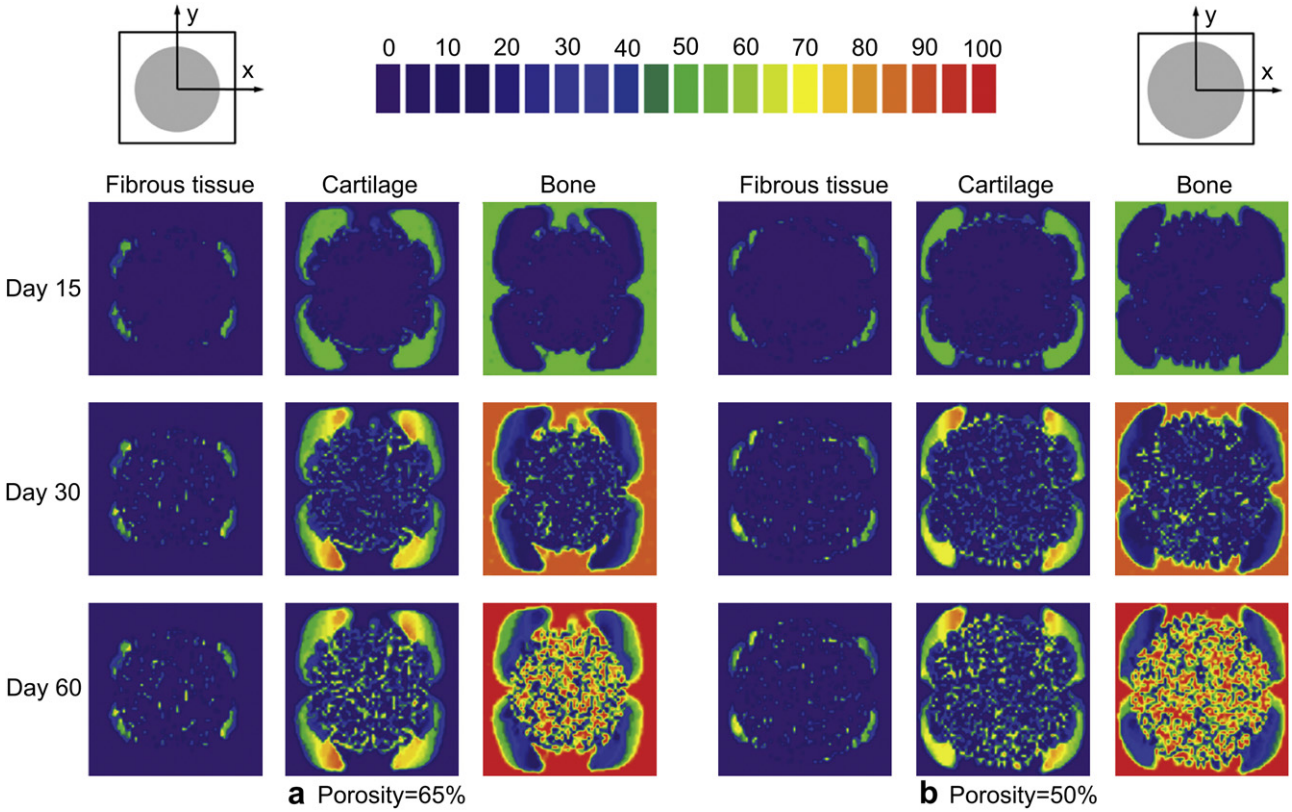

Fig. 3. The mechanobiological evolutions of PLGA scaffold in the strut frames with circular cross-sections. Upper-left and right schematic diagrams shows the configuration of scaffold RVE (dark region represents polymer matrix). (a) Porosity = 65%. (b) Porosity = 50%.

determining the mechanobiological stimulus S as defined in Eq. (10)) within similar scaffold architectures. In the highest porosity case (80% as in Fig. 2(b)), majority of bony tissue distributes at the peripheral region. While in the low porosity cases (Fig. 3), a considerable portion of neo-bone is regenerated inside the hydrolyzed voids.

For the biodegradable scaffold, it is expected that the regenerated tissues can gradually replace the degraded scaffold matrix and maintain the multi-functionality, e.g. mechanical support and fluidic transport, during degradation and regeneration. Hence, the effective properties are of particular importance in characterizing the performance of tissue-scaffold systems. By applying the homogenization procedure on RVE construct as given in Eqs. (1,2), the evolutions of normalized effective properties (i.e. the macroscopic properties of the entire scaffold structure), specifically, mechanical stiffness and fluidic permeability, are plotted in Fig. 4. Since there is no tissue differentiation taking place in the first 7 days due to the MSC maturation process, the hydrolysis reaction dominates the evolution of construct. As a result, the effective mechanical stiffness gradually decreases in the first 20 days (Fig. 4(a,c)). As neo-tissue becomes mature and acts as load-bearing tissue, the effective stiffness of entire tissue-scaffold systems gradually increases in particular after 50 days, finally approaching the maxima at day 75. On the other hand, as shown in Fig. 4(b) and (d), the effective permeability in the both cases increases significantly after day 8 and gradually approaches their maxima around 35–40 days. The time difference of reaching the corresponding maxima of the effective stiffness and permeability is mainly due to the cell maturation process, where the existing study has shown that the elasticity modulus of cells during maturation process increases exponentially with time (60 days to reach the maximum in this study), while the permeable capacity of cells exhibits little change during maturation [53]. In addition, from Table 1, it is found that the shear stiffness appears more strengthened than the normal components in the both x and y directions. By day 70, the stiffness component in the x direction is approximately two times higher than that in the y direction due to the mono-directional external loading applied.

Regarding the role of scaffold configuration on the regenerative process (Fig. 4(a,b) and Table 1), it should be noted that the effective normal stiffness in the y direction is much higher in the rectangular scaffold than that in the circular scaffold, while the x-directional normal and shear components have no distinct differences. Moreover, the effective permeabilities in x and y directions are both higher in the rectangular scaffold than those in the circular scaffold for the same porosity (80%). Concerning the role of scaffold porosity, as shown in Fig. 4(c,d) and Table 1, it can be observed that the effective stiffness components C_{xx} and G_{xy} become higher at day 75 when the porosity decreases from 80% to 50%, whereas the initial stiffness at day 0 is much lower in the highly-porous scaffolds. Such findings raise a vital yet challenging issue for scaffold micro-architecture design, i.e. how to choose the porosity/architecture to maintain the desired effective properties during degradation and regeneration. If the porosity in initial scaffold architecture is too high, the use of less polymeric material may lead to a lower effective stiffness in the early stage of regeneration process, which may not be preferable for supporting external mechanical loading and stimulating tissue regeneration. On the other hand, a higher porosity provides a higher effective permeability, which may better promote bony tissue generation. Consequentially, the effective stiffness could be even higher after regeneration. Thus, the ongoing effective properties of tissue-scaffold construct over the entire regenerative process seem more indicative for evaluating the performance of scaffold designs.

Please cite this article in press as: Chen Y, et al., Microstructure design of biodegradable scaffold and its effect on tissue regeneration, Biomaterials (2011), doi:10.1016/j.biomaterials.2011.03.064

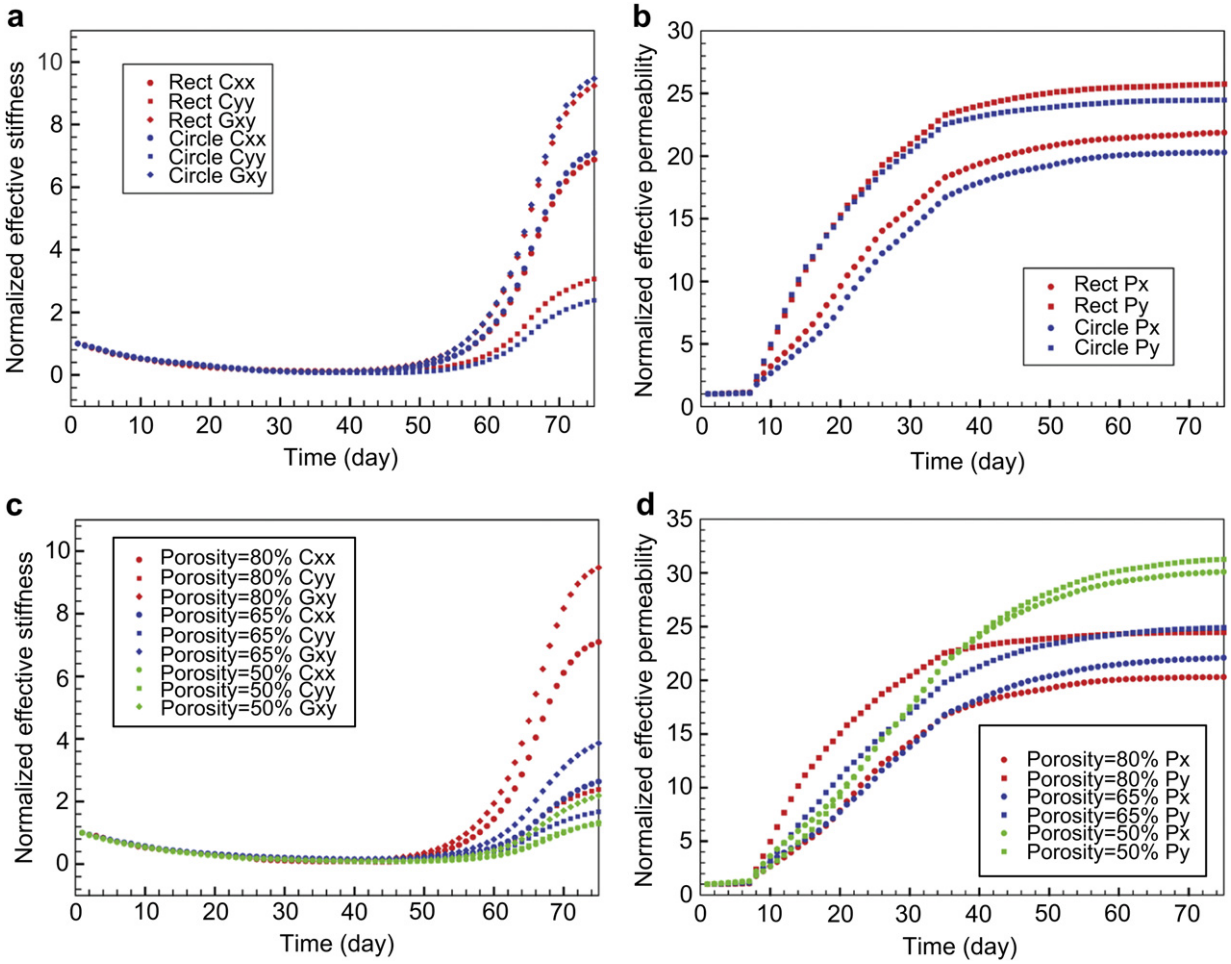

Fig. 4. The normalized effective mechanical stiffness and fluidic permeability of different scaffolds during regenerative process. (a–b) Scaffolds with rectangular and circular cross-sections (porosity = 80%). (c–d) Scaffolds with circular cross-section in 80% 65% and 50% porosities.

Furthermore, Fig. 5 shows the percentages of various cell phenotypes in different scaffold designs. Comparing the cell percentages in different configurations, it is found that the circular scaffold generates more cartilage than the rectangular one. There is also a notable difference in bone formation at day 60. As illustrated in Fig. 5(b), the porosity also plays an important role in determining the scaffold performance. When the scaffolds have the same configuration, increase in porosity would lead to a larger percentage of bone formation, which correlates to the findings in effective stiffness as shown in Fig. 4(c).

3.2. 3D models: optimized scaffold micro-architectures

3.2.1. Multi-objective topology optimization of scaffold micro-architecture

As aforementioned, scaffold should provide a desirable biomechanical environment with a sufficient mechanical support and biological network for the functional tissues to be generated *in vitro* or *in vivo*. Following the formulation of maximizing the stiffness and permeability as in Eq. (3), a multi-objective topology optimization for biphasic base-cell micro-architectures is carried out in

Table 1
The initial and ultimate effective properties of different scaffold networks.

	Rectangular Cross-section (80%)		Circular Cross-section (80%)		Circular Cross-section (65%)		Circular Cross-section (50%)	
	Day 0	Day 75	Day 0	Day 75	Day 0	Day 75	Day 0	Day 75
Stiffness C_{xx}	186.82	1302.2	184.22	1297.5	347.59	979.04	500.25	742.07
Stiffness C_{yy}	186.69	605.09	184.18	463.53	347.59	622.56	500.25	694.60
Stiffness G_{xy}	46.724	437.40	46.053	436.79	86.925	359.43	125.13	301.84
Permeability P_x	0.8548	25.111	0.8603	24.213	0.7500	22.787	0.6590	22.450
Permeability P_y	0.8544	27.943	0.8605	27.052	0.7524	24.654	0.6614	23.548

Please cite this article in press as: Chen Y, et al., Microstructure design of biodegradable scaffold and its effect on tissue regeneration, Biomaterials (2011), doi:10.1016/j.biomaterials.2011.03.064

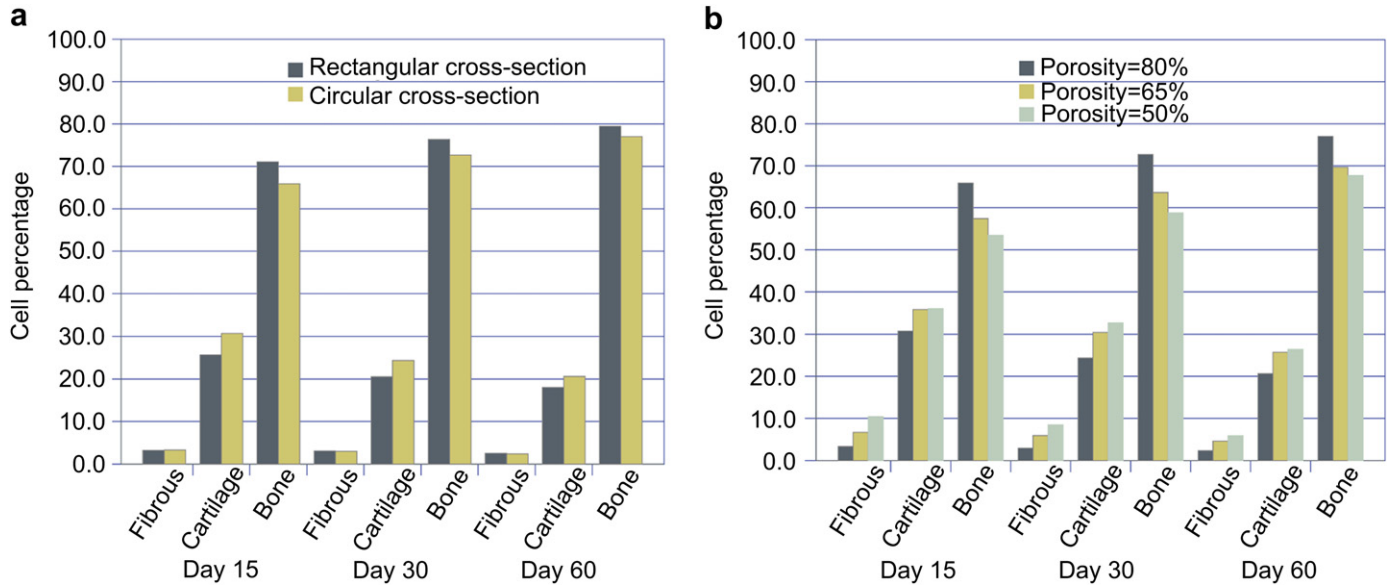

Fig. 5. Percentages of cell phenotypes during regeneration within the different scaffolds. (a) Scaffolds with rectangular and circular cross-sections (porosity = 80%). (b) Scaffolds with circular cross-sections (porosity = 80%, 65% and 50% respectively).

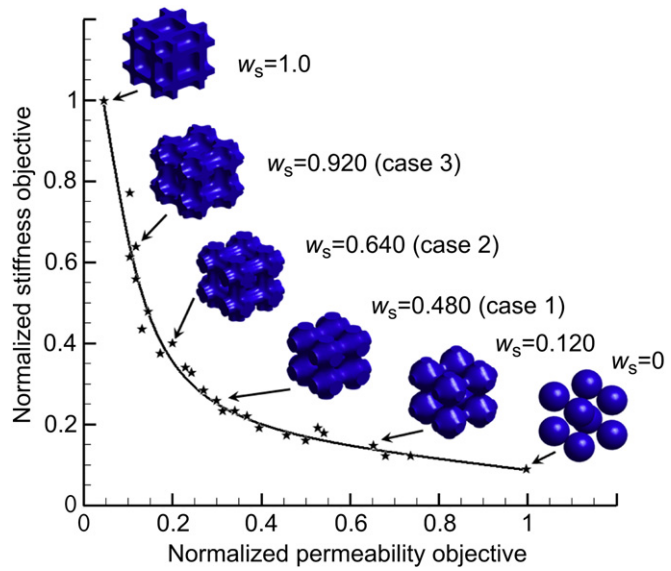

Fig. 6. Pareto front of the 3D biphasic multi-objective topology optimization of scaffold micro-architecture. Six representative designs with different w_s are shown, where the polymer phase is displayed. Three cases in different effective properties are chosen for further investigations (case 1: $w_s = 0.48$; case 2: $w_s = 0.64$; case 3: $w_s = 0.92$).

this section. Typically, the Young's modulus (E) of scaffold matrix (solid phase) made of biodegradable polymer material is significantly higher than that of the biological substances such as granulation tissue in the 'void phase', while the permeability (P) exhibits an opposite behavior. We adopt the dimensionless Young's modulus and permeability as per the factors of the differences between polymer and biological substance (specifically, $E_1 = 1000$ and $P_1 = 1$ for scaffold phase; $E_2 = 1$ and $P_2 = 1000$ for pore phase) to represent the relative material properties for the biphasic optimization [5]. By changing two weighting factors w_s and w_p in Eq. (3), a series of optimal base-cell structures ($V_c = 60\%$) with different effective properties can be obtained as shown in the normalized Pareto plot in Fig. 6. It is clear that the strong competition between stiffness and permeability criteria creates a convex Pareto front when changing the weighting factor w_s from 0 to 1 with an increment of 0.04. In this exercise, the normalizing parameter C^* is chosen as the effective stiffness with $w_s = 1$, while P^* is the effective permeability with $w_s = 0$. For a full permeability design ($w_s = 0$), the scaffold material (blue/dark) is isolated by permeable substance and forms some periodic polymeric spheres to maximize fluidic transport. As w_s increases, stiffer material gradually forms a scaffolding architecture to enhance the mechanical support. When $w_s = 1$ (the full stiffness design), an orthogonal structure emerges to maximize the stiffness.

In tissue engineering, both stiffness and permeability criteria are important. On the one hand, numerous studies have shown that the mechanical stiffness of scaffold should match or at least be within a certain allowable range of host tissue [1], meaning that the tissue-scaffold system should bear the external loading properly to avoid either mechanical failure or stress shielding. On the other hand, the scaffold should provide a cell-favored environment allowing transporting oxygen/nutrients and metabolites. Nevertheless, how to balance these two criteria for better regenerative outcome necessitates further detailed studies. It is noted that the scaffolds with a higher w_s (e.g. $w_s > 0.92$) have insufficient permeability, while those with a lower w_s (i.e. $w_s < 0.48$) exhibit rather weak scaffolding connectivity; both should not be considered here. We thus choose three representative scaffold RVEs from the Pareto

Table 2
Three representative scaffold architectures to be further investigated in degradation and mechano-regulatory tissue regeneration models.

	w_s/w_p	Initial effective stiffness ($C_{xx}/C_{yy}/C_{zz}/G_{xy}/G_{yz}/G_{xz}$)	Initial effective permeability ($P_x/P_y/P_z$)
Case 1	0.48/0.52	282.51/281.36/282.53/64.97/65.01/65.18	0.6253/0.6247/0.6253
Case 2	0.64/0.36	301.37/301.11/300.67/66.73/66.75/66.39	0.5703/0.5700/0.5797
Case 3	0.92/0.08	320.47/321.41/322.04/70.78/71.40/71.07	0.5096/0.5106/0.5108

Please cite this article in press as: Chen Y, et al., Microstructure design of biodegradable scaffold and its effect on tissue regeneration, Biomaterials (2011), doi:10.1016/j.biomaterials.2011.03.064

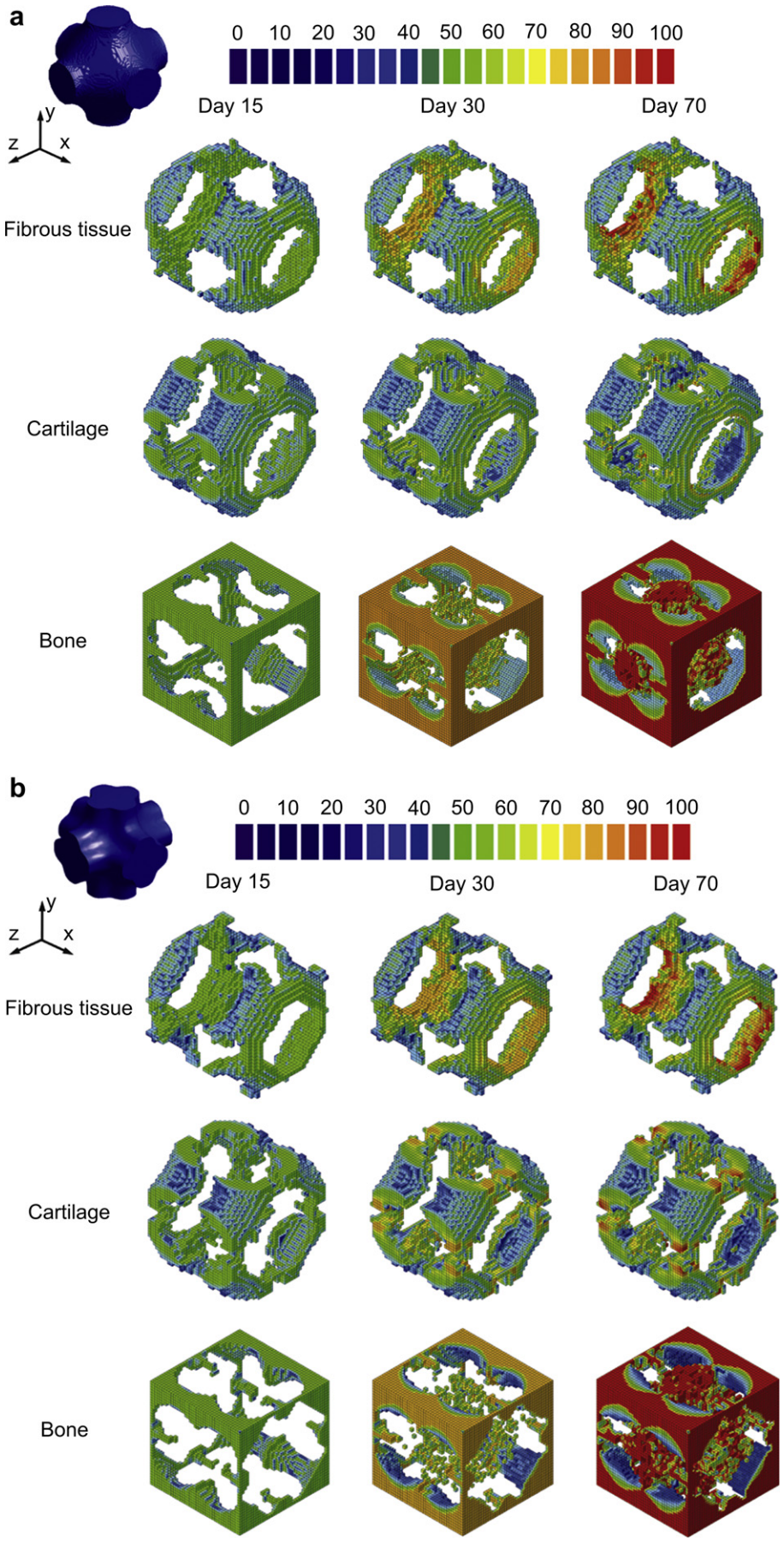

Fig. 7. The mechanobiological evolutions of different scaffold architectures for three representative cases (porosity = 40%). (a) Case 1. (b) Case 2. (c) Case 3.

Please cite this article in press as: Chen Y, et al., Microstructure design of biodegradable scaffold and its effect on tissue regeneration, Biomaterials (2011), doi:10.1016/j.biomaterials.2011.03.064

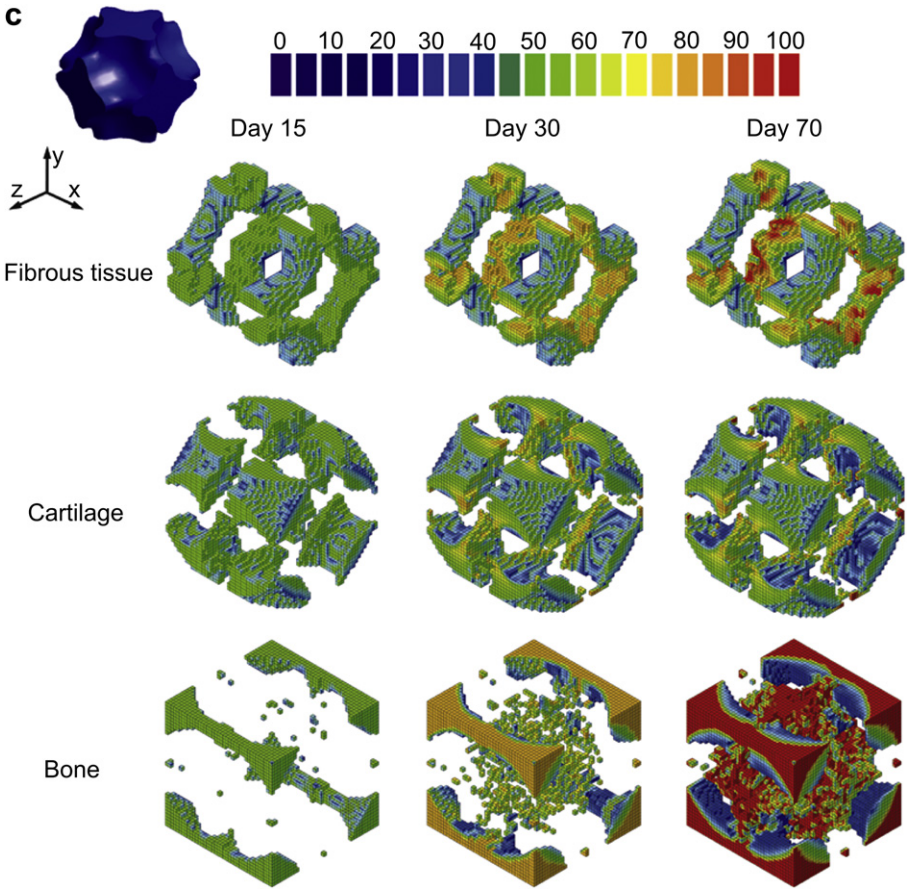

Fig. 7. (*continued*).

front in Fig. 6 (i.e. $w_s = 0.48$, 0.64 and 0.92, whose effective properties are listed in Table 2), to examine their tissue regenerative capabilities subject to degradation, thereby exploring the roles of stiffness and permeability criteria in the design of scaffold micro-architecture.

3.2.2. Tissue regeneration in optimal scaffold micro-architectures

Based on the abovementioned multi-objective topology optimization, three representative scaffold micro-architectural designs are further explored by the polymeric degradation and mechano-regulatory tissue regeneration models herein. Firstly, the micro-architectural evolutions of tissue-scaffold systems during regeneration are examined. Fig. 7 shows the neo-tissue growth in different scaffold designs. It can be seen that in these three cases, majority of fibroblasts is formed in the region close to the polymer matrix in the beginning. As the matrix material degrades, MSCs start penetrating into the polymer voids, where neo-tissue can be generated as long as the nutrients can sufficiently diffuse through. When most of the scaffold matrix is degraded after 70 days, the initial polymer phase is mainly occupied by newly-generated tissues. It should be mentioned that, to better show the distribution of different cell phenotypes, only the elements with relative cell density higher than 20% are displayed in Fig. 7. Nevertheless, in all these three cases, neo-tissues are gradually substituting the hydrolyzed scaffold matrix. In the beginning, MSCs that are close to the surface of scaffold differentiate first. As the hydrolysis reaction of polymer matrix evolves, more voids are generated in the bulk of scaffold. Therefore, MSCs enter into those voids through migration and proliferation, followed by cellular maturation and further mechano-regulatory activities. As such, newly-generated tissues would considerably take the load-bearing capacity that the original scaffold structure has.

Based upon these three different ratios of stiffness/permeability criteria, the micro-architectural design plays a certain role in determining the regenerative pattern and layout of cell phenotypes, thus affecting the effective properties of tissue-scaffold systems. For case 1 ($w_s = 0.48$) (Fig. 7(a)), despite a lower initial effective stiffness (Table 2), the distribution of regenerated osteoblasts exhibits a good connectivity due to sufficient permeability, leading to a better interconnected bony structure. As w_s increases, lower permeability (e.g. Case 3 as illustrated in Fig. 7(c)) results in some disconnected neo-bony tissue in the lateral (y and z) directions, which would weaken the effective stiffness and strength in those directions when the scaffold further degrades.

Fig. 8 illustrates the evolutions of effective stiffness and permeability during scaffold degradation and tissue ingrowth. Due to the double-symmetry of scaffold micro-architectures under compressive loading along the x axis, the effective stiffness and permeability tensors are almost double-symmetrical (despite the random characteristics of degradation model), i.e. the components are the same in the y and z directions but different in the x direction. In the first 20 days, since the hydrolysis is weakening the polymeric matrix, all components of effective stiffness decrease. As neo-tissues develop, the normal and shear effective stiffnesses of entire tissue-scaffold system gradually increase. Regarding the effective permeability, all the components remain almost constant in the first 7 days since the hydrolysis reaction that mainly takes place inside the polymer matrix makes less contribution to the

Please cite this article in press as: Chen Y, et al., Microstructure design of biodegradable scaffold and its effect on tissue regeneration, Biomaterials (2011), doi:10.1016/j.biomaterials.2011.03.064

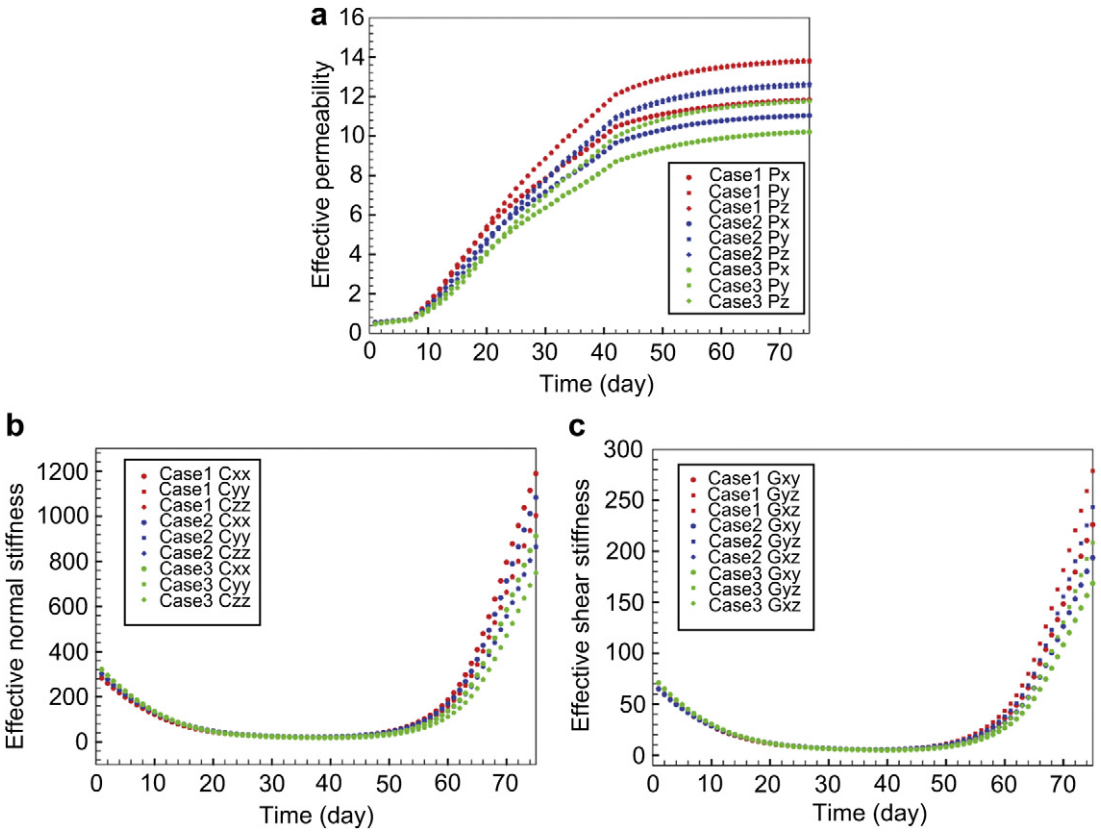

Fig. 8. The effective properties of different scaffold architectures during regenerative process. (a) Effective permeabilities of three different cases. (b–c) Effective normal and shear stiffness components.

effective permeability. As degradation evolves inside the scaffold material, the newly-generated tissue substances that have a higher permeability enhance this effective property significantly.

It is again illustrated in Fig. 8 that, the stiffness/permeability criteria for scaffold micro-architectural design have a considerable impact on the time-dependent effective properties during tissue regeneration. It can be seen from Fig. 8(b) and (c) that Case 1 ($w_s = 0.48$, which has a lower initial effective stiffness) presents higher normal and shear stiffnesses than Case 3 ($w_s = 0.92$) after 50 days and the difference widens more significantly after 70 days, which correlates to the results obtained in 2D examples. For the effective permeability, on the other hand, although the differences of initial permeabilities among these three cases as shown in Table 2 are small, almost 20% difference of effective permeability can be observed after 70 days as illustrated in Fig. 8(a). As w_s increases (e.g. from Case 1 to Case 3, i.e. more emphasis is made on the stiffness criterion), the effective permeabilities in all the three directions decrease notably. Furthermore, Fig. 9 shows the percentages of cell phenotypes in the different design cases during regeneration. It can be seen that, as the emphasis on the permeability increases (i.e. from Case 3 to Case 1), the corresponding design has more osteoblasts (approximately 15%) differentiated from MSCs.

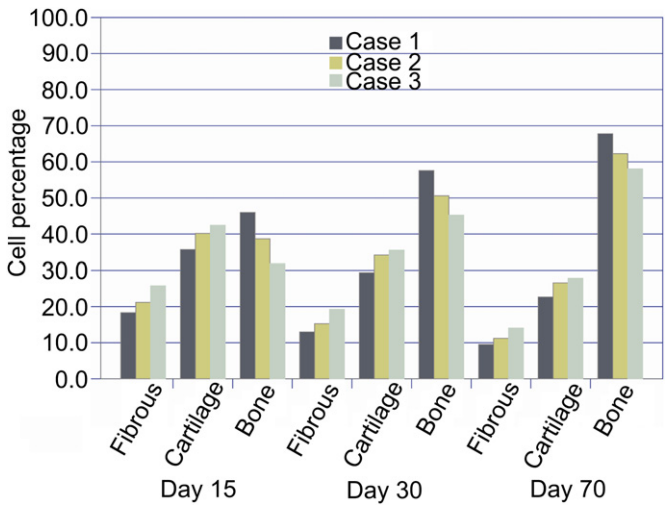

Fig. 9. Percentages of cell phenotypes during regeneration within different scaffold architectures in three representative cases.

Interestingly, it is noted that although Case 1 ($w_s = 0.48$) has a lower stiffness in the initial design due to more emphasis on the permeability design ($w_p = 0.52$), it exhibits a good connectivity of regenerated bony tissue structures, thereby presenting higher effective properties in both stiffness and permeability in the final tissue-scaffold system. Also it promotes the regenerative effectiveness and results in more bone formation than the other two cases with higher w_s. This may suggest that, as long as the scaffold stiffness meets the requirement for mechanical support, increasing the permeability of scaffold design can be useful. In other words, the permeability criterion plays a more significant role than the stiffness one to enhance the performance of scaffold micro-architecture in terms of tissue regeneration outcome.

4. Concluding Remarks

In this paper, a mathematical model was proposed to assess the role of scaffold architectures on tissue regeneration outcome by

Please cite this article in press as: Chen Y, et al., Microstructure design of biodegradable scaffold and its effect on tissue regeneration, Biomaterials (2011), doi:10.1016/j.biomaterials.2011.03.064

considering continuous polymer degradation and tissue ingrowth. Firstly, the multi-objective topology optimization was implemented to obtain a series of scaffold architectures that have different effective stiffness and permeability combinations. Secondly, the degradation of scaffold matrix is modeled as a stochastic hydrolysis process enhanced by the diffusion-controlled autocatalysis. Finally, the mechano-regulatory tissue regeneration model was employed to explore the healing process within the optimized biodegradable scaffolds. To reveal the interplay characteristics among mechanical environment, bio-chemical process and scaffold architecture, simultaneously modeling the time-dependent scaffold degradation and mechanobiological tissue regeneration is essential to evaluate the dynamic performance of scaffolds. The illustrative examples showed that the design of scaffold architecture has a significant impact on the tissue regeneration outcome in terms of the effective properties of tissue-scaffold systems via the homogenization method, thus demonstrated the necessities in compromising with the different criteria in scaffold micro-structural design, before being fabricated via rapid prototyping technique, e.g. solid free-form fabrication. Under certain stiffness, the permeability criterion seems to play a more noteworthy role in determining the regenerative performance of tissue-scaffold systems. The study on the interactive process of scaffold degradation and tissue growth provided some new insights into the micro-structural design of biodegradable scaffold for tissue engineering. Further work can be devoted to investigate the effects of both bulk degradation and surface erosion of biodegradable polymer scaffold on the mechanobiological regenerative process.

Acknowledgements

The support from the Australian Research Council (ARC) is greatly acknowledged. The first author is grateful for the Faculty scholarship at the University of Sydney.

References

[1] Sturm S, Zhou SW, Mai YW, Li Q. On stiffness of scaffolds for bone tissue engineering - a numerical study. J Biomech 2010;43:1738–44.
[2] Karande TS, Ong JL, Agrawal CM. Diffusion in musculoskeletal tissue engineering scaffolds: design issues related to porosity, permeability, architecture, and nutrient mixing. Ann Biomed Eng 2004;32(12):1728–43.
[3] Rose F, Oreffo ROC. Bone tissue engineering: hope vs hype. Biochem Biophys Res Commun 2002;292(1):1–7.
[4] Hollister SJ. Porous scaffold design for tissue engineering. Nat Mater 2005; 4(7):518–24.
[5] Hollister SJ. Scaffold design and manufacturing: from concept to clinic. Adv Mater 2009;21(32–33):3330–42.
[6] Hutmacher DW. Scaffold design and fabrication technologies for engineering tissues - state of the art and future perspectives. J Biomater Sci-Polym Ed 2001;12(1):107–24.
[7] Lacroix D, Planell JA, Prendergast PJ. Computer-aided design and finite-element modelling of biomaterial scaffolds for bone tissue engineering. Philos Trans R Soc A-Math Phys Eng Sci 1895;2009(367):1993–2009.
[8] Kang H, Lin CY, Hollister SJ. Topology optimization of three dimensional tissue engineering scaffold architectures for prescribed bulk modulus and diffusivity. Struct Multidiscip Optim 2010;45(4):633–44.
[9] Cordell JM, Vogl ML, Johnson AJW. The influence of micropore size on the mechanical properties of bulk hydroxyapatite and hydroxyapatite scaffolds. J Mech Behav Biomed Mater 2009;2(5):560–70.
[10] Karageorgiou V, Kaplan D. Porosity of 3D biornaterial scaffolds and osteogenesis. Biomaterials 2005;26(27):5474–91.
[11] Bendsoe MP, Sigmund O. Topology, optimization: theory, methods, and applications. Berlin, New York: Springer; 2003.
[12] Hollister SJ, Maddox RD, Taboas JM. Optimal design and fabrication of scaffolds to mimic tissue properties and satisfy biological constraints. Biomaterials 2002;23(20):4095–103.
[13] Lin CY, Kikuchi N, Hollister SJ. A novel method for biomaterial scaffold internal architecture design to match bone elastic properties with desired porosity. J Biomech 2004;37(5):623–36.
[14] Chen YH, Zhou SW, Li Q. Computational design for multifunctional microstructural composites. Int J Mod Phys B 2009;23(6–7):1345–51.
[15] Sanz-Herrera JA, Garcia-Aznar JM, Doblare M. On scaffold designing for bone regeneration: a computational multiscale approach. Acta Biomater 2009;5(1): 219–29.
[16] von Burkersroda F, Schedl L, Gopferich A. Why degradable polymers undergo surface erosion or bulk erosion. Biomaterials 2002;23(21):4221–31.
[17] Gopferich A. Mechanisms of polymer degradation and erosion. Biomaterials 1996;17(2):103–14.
[18] Hutmacher DW. Scaffolds in tissue engineering bone and cartilage. Biomaterials 2000;21(24):2529–43.
[19] Bawolin NK, Li MG, Chen XB, Zhang WJ. Modeling material-degradation-induced elastic property of tissue engineering scaffolds. J Biomech Eng-Trans ASME 2010;132(11).
[20] Siepmann J, Elkharraz K, Siepmann F, Klose D. How autocatalysis accelerates drug release from PLGA-based microparticles: a quantitative treatment. Biomacromolecules 2005;6(4):2312–9.
[21] Klose D, Siepmann F, Elkharraz K, Krenzlin S, Siepmann J. How porosity and size affect the drug release mechanisms from PLIGA-based microparticles. Int J Pharm 2006;314(2):198–206.
[22] Chen YH, Zhou SW, Li Q. Mathematical modeling of degradation for bulk-erosive polymers: applications in tissue engineering scaffolds and drug delivery systems. Acta Biomater 2011;7(3):1140–9.
[23] Huiskes R, Ruimerman R, van Lenthe GH, Janssen JD. Effects of mechanical forces on maintenance and adaptation of form in trabecular bone. Nature 2000;405(6787):704–6.
[24] van der Meulen MCH, Huiskes R. Why mechano-biology? a survey article. J Biomech 2002;35(4):401–14.
[25] Jacobs CR, Temiyasathit S, Castillo AB. Osteocyte mechano-biology and pericellular mechanics. Annu Rev Biomed Eng; 2010:369–400.
[26] Kelly DJ, Jacobs CR. The role of mechanical signals in regulating chondrogenesis and osteogenesis of mesenchymal stem cells. Birth Defects Res Part C-Embryo Today-Rev 2010;90(1):75–85.
[27] Carter DR, Blenman PR, Beaupre GS. Correlations between mechanical-stress history and tissue differentiation in initial fracture-healing. J Orthop Res 1988;6(5):736–48.
[28] Kelly DJ, Prendergast PJ. Mechano-regulation of stem cell differentiation and tissue regeneration in osteochondral defects. J Biomech 2005;38(7): 1413–22.
[29] Adachi T, Osako Y, Tanaka M, Hojo M, Hollister SJ. Framework for optimal design of porous scaffold microstructure by computational simulation of bone regeneration. Biomaterials 2006;27(21):3964–72.
[30] Tsubota K, Suzuki Y, Yamada T, Hojo M, Makinouchi A, Adachi T. Computer simulation of trablecular remodeling in human proximal femur using large-scale voxel FE models: approach to understanding Wolff's law. J Biomech 2009;42(8):1088–94.
[31] Prendergast PJ, Huiskes R, Soballe K. Biophysical stimuli on cells during tissue differentiation at implant interfaces. J Biomech 1997;30(6):539–48.
[32] Byrne DP, Lacroix D, Planell JA, Kelly DJ, Prendergast PJ. Simulation of tissue differentiation in a scaffold as a function of porosity, Young's modulus and dissolution rate: application of mechano-biological models in tissue engineering. Biomaterials 2007;28(36):5544–54.
[33] Stops AJF, Heraty KB, Browne M, O'Brien FJ, McHugh PE. A prediction of cell differentiation and proliferation within a collagen-glycosaminoglycan scaffold subjected to mechanical strain and perfusive fluid flow. J Biomech 2010;43(4): 618–26.
[34] Checa S, Prendergast PJ. A mechano-biological model for tissue differentiation that includes angiogenesis: a lattice-based modeling approach. Ann Biomed Eng 2009;37(1):129–45.
[35] Sun W, Darling A, Starly B, Nam J. Computer-aided tissue engineering: overview, scope and challenges. Biotechnol Appl Biochem 2004;39:29–47.
[36] Volkmer E, Drosse I, Otto S, Stangelmayer A, Stengele M, Kallukalam BC, et al. Hypoxia in static and dynamic 3D culture systems for tissue engineering of bone. Tissue Eng Part A 2008;14(8):1331–40.
[37] Guest JK, Prevost JH. Optimizing multifunctional materials: design of microstructures for maximized stiffness and fluid permeability. Int J Solids Struct 2006b;43(22–23):7028–47.
[38] McIntosh L, Cordell JM, Johnson AJW. Impact of bone geometry on effective properties of bone scaffolds. Acta Biomater 2009;5(2):680–92.
[39] de Kruijf N, Zhou SW, Li Q, Mai YW. Topological design of structures and composite materials with multiobjectives. Int J Solids Struct 2007;44(22–23): 7092–109.
[40] Chen YH, Zhou SW, Li Q. Multiobjective topology optimization for finite periodic structures. Comput Struct 2010;88(11–12):806–11.
[41] Guest JK, Prevost JH. Design of maximum permeability material structures. Comput Meth Appl Mech Eng 2007;196(4–6):1006–17.
[42] Gopferich A. Polymer bulk erosion. Macromolecules 1997;30(9):2598–604.
[43] Tracy MA, Ward KL, Firouzabadian L, Wang Y, Dong N, Qian R, et al. Factors affecting the degradation rate of poly(lactide-co-glycolide) microspheres in vivo and in vitro. Biomaterials 1999;20(11):1057–62.
[44] Papoulis A. Probability, random variables and stochastic processes. 3rd ed. McGraw-Hill Companies; 1991.
[45] Grizzi I, Garreau H, Li S, Vert M. Hydrolytic degradation of devices based on poly(DL-lactic acid) size dependence. Biomaterials 1995;16(4):305–11.
[46] Lam CXF, Savalani MM, Teoh SH, Hutmacher DW. Dynamics of in vitro polymer degradation of polycaprolactone-based scaffolds: accelerated versus simulated physiological conditions. Biomed Mater 2008;3(3).

Please cite this article in press as: Chen Y, et al., Microstructure design of biodegradable scaffold and its effect on tissue regeneration, Biomaterials (2011), doi:10.1016/j.biomaterials.2011.03.064

[47] Thombre AG, Himmelstein KJ. A simultaneous transport-reaction model for controlled drug delivery from catalyzed bioerodible polymer matrices. Aiche J 1985;31(5):759–66.
[48] Huiskes R, VanDriel WD, Prendergast PJ, Soballe K. A biomechanical regulatory model for periprosthetic fibrous-tissue differentiation. J Mater Sci-Mater Med 1997;8(12):785–8.
[49] Neogi P. Diffusion in polymers. New York: Marcel Dekker; 1996.
[50] Gibson LJ. The mechanical-behavior of cancellous bone. J Biomech 1985;18(5):317. -&.
[51] Isaksson H, van Donkelaar CC, Huiskes R, Ito K. A mechano-regulatory bone-healing model incorporating cell-phenotype specific activity. J Theor Biol 2008;252(2):230–46.
[52] Hutmacher DW, Sittinger M, Risbud MV. Scaffold-based tissue engineering: rationale for computer-aided design and solid free-form fabrication systems. Trends Biotechnol 2004;22(7):354–62.
[53] Boccaccio A, Prendergast PJ, Pappalettere C, Kelly DJ. Tissue differentiation and bone regeneration in an osteotomized mandible: a computational analysis of the latency period. Med Biol Eng Comput 2008;46(3):283–98.

Please cite this article in press as: Chen Y, et al., Microstructure design of biodegradable scaffold and its effect on tissue regeneration, Biomaterials (2011), doi:10.1016/j.biomaterials.2011.03.064